Since January 2020 Elsevier has created a COVID-19 resource centre with free information in English and Mandarin on the novel coronavirus COVID-19. The COVID-19 resource centre is hosted on Elsevier Connect, the company's public news and information website.

Elsevier hereby grants permission to make all its COVID-19-related research that is available on the COVID-19 resource centre - including this research content - immediately available in PubMed Central and other publicly funded repositories, such as the WHO COVID database with rights for unrestricted research re-use and analyses in any form or by any means with acknowledgement of the original source. These permissions are granted for free by Elsevier for as long as the COVID-19 resource centre remains active.

Article

Structure

A monoclonal antibody against staphylococcal enterotoxin B superantigen inhibits SARS-CoV-2 entry *in vitro*

Graphical abstract

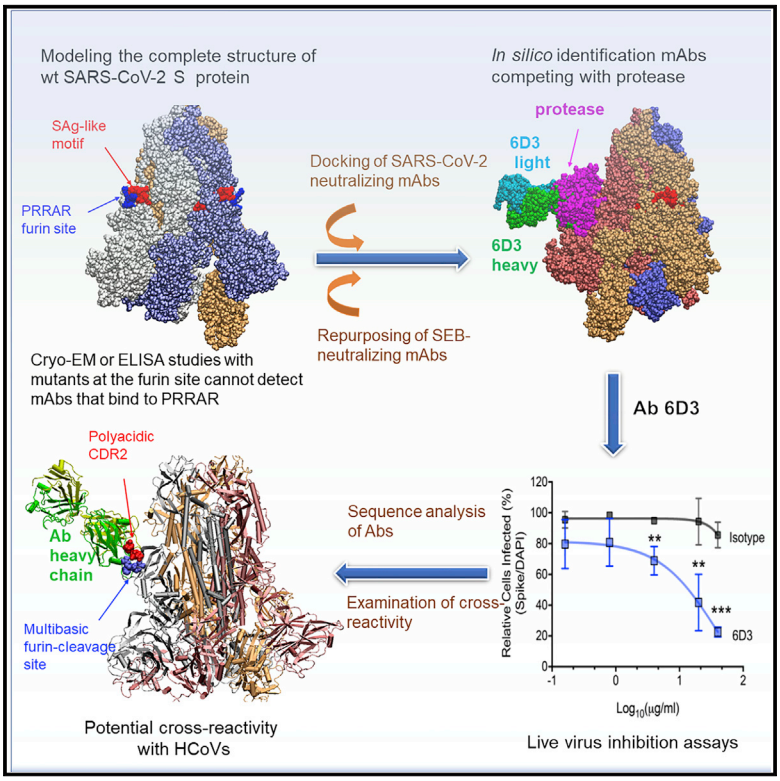

Highlights

- Modeling predicted anti-SEB mAb, 6D3, to cross-react with the SARS-CoV-2 spike
- Live virus assays demonstrated that 6D3 effectively blocks SARS-CoV-2 viral entry
- 6D3 binds the S1/S2 site, interfering with the proteolytic activity of TMPRSS2/furin
- An acidic residue cluster at 6D3 VH enables strong binding to the polybasic S1/S2 site

Authors

Mary Hongying Cheng, Rebecca A. Porritt, Magali Noval Rivas, ..., Bettina C. Fries, Moshe Arditi, Ivet Bahar

Correspondence

moshe.arditi@cshs.org (M.A.), bahar@pitt.edu (I.B.)

In brief

Cheng et al. demonstrate that an anti-SEB antibody can bind the SARS-CoV-2 polybasic (PRRA) insert to inhibit infection in live virus assays. The overlap between the superantigenic site of the spike and its proteolytic cleavage site suggests that the mAb prevents viral entry by interfering with the proteolytic activity of cell proteases.

Cheng et al., 2021, Structure *29*, 951–962
September 2, 2021 © 2021 Elsevier Ltd.
https://doi.org/10.1016/j.str.2021.04.005

Structure

CellPress

Article

A monoclonal antibody against staphylococcal enterotoxin B superantigen inhibits SARS-CoV-2 entry *in vitro*

Mary Hongying Cheng,[1] Rebecca A. Porritt,[2,3] Magali Noval Rivas,[2,3] James M. Krieger,[1] Asli Beyza Ozdemir,[2,3] Gustavo Garcia, Jr.,[4,5] Vaithilingaraja Arumugaswami,[4,5] Bettina C. Fries,[6,7] Moshe Arditi,[2,3,8,*] and Ivet Bahar[1,8,9,*]

[1]Department of Computational and Systems Biology, School of Medicine, University of Pittsburgh, Pittsburgh, PA 15213, USA

[2]Department of Pediatrics, Division of Pediatric Infectious Diseases and Immunology, Cedars-Sinai Medical Center, Los Angeles, CA 90048, USA

[3]Biomedical Sciences, Infectious and Immunologic Diseases Research Center, Cedars-Sinai Medical Center, Los Angeles, CA 90048, USA

[4]Department of Molecular and Medical Pharmacology, David Geffen School of Medicine, University of California, Los Angeles, Los Angeles, CA 90095, USA

[5]Eli and Edythe Broad Center of Regenerative Medicine and Stem Cell Research, University of California, Los Angeles, Los Angeles, CA 90095, USA

[6]Department of Medicine, Stony Brook University Hospital, Stony Brook, New York, NY 11794, USA

[7]Northport VA Medical Center, Northport, NY 11768, USA

[8]These authors contributed equally

[9]Lead contact

*Correspondence: moshe.arditi@cshs.org (M.A.), bahar@pitt.edu (I.B.)

https://doi.org/10.1016/j.str.2021.04.005

SUMMARY

We recently discovered a superantigen-like motif sequentially and structurally similar to a staphylococcal enterotoxin B (SEB) segment, near the S1/S2 cleavage site of the SARS-CoV-2 spike protein, which might explain the multisystem inflammatory syndrome (MIS-C) observed in children and the cytokine storm in severe COVID-19 patients. We show here that an anti-SEB monoclonal antibody (mAb), 6D3, can bind this viral motif at its polybasic (PRRA) insert to inhibit infection in live virus assays. The overlap between the superantigenic site of the spike and its proteolytic cleavage site suggests that the mAb prevents viral entry by interfering with the proteolytic activity of cell proteases (furin and TMPRSS2). The high affinity of 6D3 for this site originates from a polyacidic segment at its heavy chain CDR2. The study points to the potential utility of 6D3 for possibly treating COVID-19, MIS-C, or common colds caused by human coronaviruses that also possess a furin-like cleavage site.

INTRODUCTION

Severe acute respiratory syndrome coronavirus 2 (SARS-CoV-2) can cause severe interstitial pneumonia with hyperinflammation (Tay et al., 2020; Vabret et al., 2020), as well as many extrapulmonary manifestations (Gupta et al., 2020), referred to as coronavirus disease 2019 (COVID-19). A novel multisystem inflammatory syndrome (MIS), reported in both children (MIS-C) and adults (MIS-A), has been observed in patients that either tested positive for or had epidemiological links to COVID-19 (Belhadjer et al., 2020; Cheung et al., 2020; Riphagen et al., 2020; Verdoni et al., 2020). MIS-C manifests as persistent fever and hyperinflammation with multiorgan involvement (Belhadjer et al., 2020; Cheung et al., 2020; Riphagen et al., 2020; Verdoni et al., 2020). The clinical similarity between MIS-C/A and toxic shock syndrome (TSS) caused by bacterial superantigens (SAgs) led to the hypothesis that SARS-CoV-2 might possess a SAg-like motif that triggers hyperinflammation (Cheng et al., 2020; Noval Rivas et al., 2020). Comparison with bacterial toxins indeed revealed a motif in the SARS-CoV-2 spike (or S) protein, the sequence and structure of which highly resemble a segment of a bacterial SAg, staphylococcal enterotoxin B (SEB). The SAg-like character of the S protein was further supported by the T cell receptor (TCR) skewing typical of the reaction to SAgs, which was observed in severe COVID-19 patients (Cheng et al., 2020).

The location of the SAg-like motif in the S protein is worthy of attention. SARS-CoV-2 S is a homotrimer, similar to other spike proteins on viruses belonging to the family of human coronaviruses (HCoVs), which includes SARS-CoV and Middle East respiratory syndrome (MERS) as well as the common cold HCoVs NL63, 229E, OC43, and HKU1 (Coutard et al., 2020; Cui et al., 2019; Forni et al., 2017). Each HCoV S protomer is composed of two subunits, S1 and S2, playing different roles in viral infection. S1 contains the receptor-binding domain (RBD) that binds to the host cell receptor (human angiotensin-converting enzyme 2 [ACE2] for SARS-CoV-2, SARS-CoV, and HCoV-NL63) (Benton

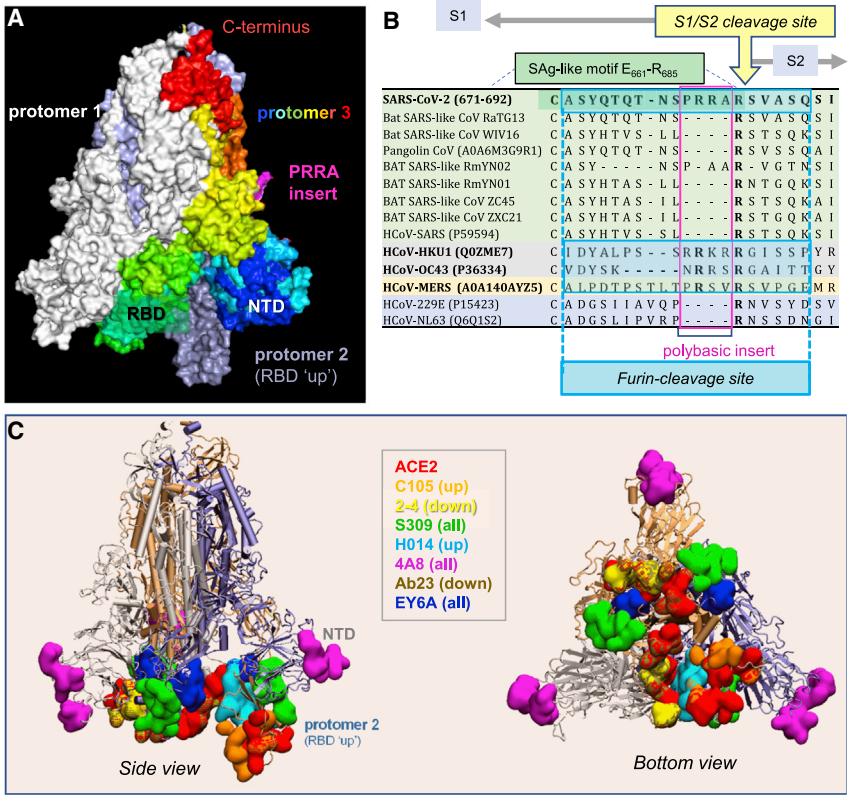

Figure 1. SARS-CoV-2 spike (S) glycoprotein structure, sequence alignment against other CoVs, and interaction sites observed in cryo-EM studies with neutralizing antibodies

(A) SARS-CoV-2 S trimer in the pre-fusion state. Protomers 1 and 2 are in white and light blue, respectively, and protomer 3 is in spectral colors from blue (N-terminal domain, NTD; residues 1–305) to red (C terminus), except for the $_{681}$PRRA$_{684}$ insert in magenta. The insert was modeled using SWISS-MODEL (Waterhouse et al., 2018). Each protomer's RBD (residues 331–524) can assume an up or down conformation in the respective receptor-bound and unbound state.

(B) Sequence alignment of SARS-CoV-2 near the S1/S2 cleavage site against multiple bat and pangolin SARS-related strains and other HCoVs, adjusted following previous studies (Coutard et al., 2020; Zhou et al., 2020b). Viruses belonging to the same lineage are shown by the same color shade, and HCoVs that encode furin-like cleavage sites are highlighted in bold font. Note that the polybasic insert PRRA of SARS-CoV-2 S is not found in closely related SARS-like CoVs but exists in MERS and HCoVs HKU1 and OC43. The furin-like cleavage site is indicated by the blue-shaded box.

(C) Side (left) and bottom (right) views of receptor (ACE2)- and antibody-binding sites observed in cryo-EM structures resolved for the S protein complexed with the ACE2 and/or various antibodies. The S trimer is shown in cartoons with a light blue protomer in the RBD-up conformation and gray and light orange protomers in the RBD-down conformation. Binding sites for ACE2 and antibodies C105 (Barnes et al., 2020), 2-4 (Liu et al., 2020), S309 (Pinto et al., 2020), H014 (Lv et al., 2020b), 4A8 (Chi et al., 2020), Ab23 (Cao et al., 2020b), and EY6A (Zhou et al., 2020a) are shown in space-filling surfaces in different colors (see the code in the inset). See Table 1 for additional details.

et al., 2020; Hoffmann et al., 2020; Matsuyama et al., 2020; Shang et al., 2020; Walls et al., 2020; Wrapp et al., 2020; Yan et al., 2020), whereas S2 contains the fusion peptide required for viral entry (Coutard et al., 2020; Cui et al., 2019; Forni et al., 2017). The SAg-like motif (residues E661–R685) lies at the C terminus of S1 (Cheng et al., 2020), at the boundary with S2. Membrane fusion requires two successive cleavages by host cell proteases, one at the S1/S2 interface (peptide bond R685↑S686), and the other at S2′ (R815↑S816) (Coutard et al., 2020; Hoffmann et al., 2020; Matsuyama et al., 2020; Shang et al., 2020; Walls et al., 2020; Wrapp et al., 2020; Yan et al., 2020). Thus, the SAg-like region overlaps the S1/S2 cleavage site of the S protein (Figures 1A and 1B).

Another interesting feature at the SAg-like region is a unique insertion, $_{681}$PRRA$_{684}$, immediately neighboring the cleavage site R685↑S686 (Figure 1A). Loss of these four residues in a mutant ΔPRRA has been recently shown to attenuate SARS-CoV-2 pathogenesis (Johnson et al., 2021). SARS-CoV-2 is the only member of the SARS family of β-coronaviruses (βCoVs) that has such an insertion (see nine such members sequentially aligned in Figure 1B, top nine rows), despite its high sequence similarity with other members of this genus (>80% sequence identity with SARS-CoV). Interestingly, MERS and common cold HKU1 and OC43 S proteins have a similar insertion at that position, despite their low (30%–40%) overall sequence identity with respect to SARS-CoV-2 spike (Figure 1B). The PRRA insert is highly flexible and, together with the adjacent arginine, the segment $_{681}$PRRAR$_{685}$ forms a highly reactive site. It plays a role in recognizing and binding the host cell proteases transmembrane protease serine 2 (TMPRSS2) and furin, whose cleavage activity is essential to S protein priming (Hoffmann et al., 2020; Shang et al., 2020; Walls et al., 2020; Wrapp et al., 2020). Recent studies further showed the role of the S1/S2 site in potentiating infectivity upon binding to the host cell co-receptor neuropilin-1 (Cantuti-Castelvetri et al., 2020; Daly et al., 2020), and our simulations revealed its propensity to bind TCRs (Cheng et al., 2020).

We hypothesized that this polybasic site, $_{681}$PRRAR$_{685}$, could thus serve as a target for SARS-CoV-2 S-neutralizing antibodies (Abs). Most SARS-CoV-2 S Abs under investigation target the RBD (and some, the N-terminal domain, NTD) (Cao et al., 2020b; Chi et al., 2020; Hansen et al., 2020; Pinto et al., 2020; Renn et al., 2020; Shi et al., 2020; Yuan et al., 2020). Figure 1C illustrates the S-protein epitopes (colored surfaces) that have been observed by cryoelectron microscopy (cryo-EM) to bind monoclonal Abs (mAbs) and ACE2 molecules. The Abs bind various poses/sites depending on the up or down state of the RBDs and their specific sequences (see Table 1). However, we note that most of these cryo-EM studies were conducted with variants in which the polybasic segment $_{682}$RRAR$_{685}$ had been replaced by GSAS or SGAG (Barnes et al., 2020; Cao et al., 2020b; Chi et al., 2020; Liu et al., 2020; Lv et al., 2020b; Pinto et al., 2020; Zhou et al., 2020a; Zost et al., 2020). Therefore, the ability, if any, of wild-type S protein to bind an Ab near the PRRA insert or the S1/S2 cleavage site may have eluded these experiments. Identification of alternative binding sites for

CellPress

Table 1. Antibody-bound complexes resolved by cryo-EM for SARS-CoV-2 spike mutants

Binding domain (conformation)	Mechanism of action	SARS-CoV-2 Ab (PDB IDs)[a]	Mutation at "RRAR"	Epitope on SARS2 spike[b]	Reference
RBD (up)	sterically hinders ACE2 binding	C105 (6XCN, 6XCM)	SGAG	D405,T415, G416, K417, Y421, Y453, F456, R457, K458, N460, Y473, A475, G476, F486, N487, G502, Y505	Barnes et al., 2020
RBD (down)	blocks ACE2-binding interface of RBD	2-4 (6XEY)	GSAS	Y449, Y453, L455, F456, V483, E484, G485, F486, Y489, F490, L492, Q493, S494	Liu et al., 2020
RBD (up/down) distinct from ACE2 binding sites	Ab-dependent cell cytotoxicity and phagocytosis	S309 (6WPT, 6WPS)	SGAG	N334, L335, P337, G339, E340, N343, A344,T345, R346, K356, R357, S359, N360, C361, L441, N343 glycan	Pinto et al., 2020
RBD (up)	blocks ACE2 binding and attachment to host cell	H014 (7CAI, 7CAC, 7CAB, 7CAK,7CAH)	GSAS	Y369, A372,S373, F374, S375, T376, F377, K378, C379, Y380, V382, S383, P384, T385, D405, V407, R408, A411, P412, Q414, N437, V503	Lv et al., 2020b
NTD (up/down)	restrains S protein structural changes	4A8 (7C2L)	GSAS	Y144, Y145, H146, K147, K150, W152, H245, R246, S247, Y248, L249	Chi et al., 2020
RBD/NTD (down)	blocks ACE2 binding	Ab23 (7BYR)	GSAS	G446, Y449, E484, G485, F486, Y489, F490, L492, Q493, S494, G496, Q498 N501, Y505, N165 glycan	Cao et al., 2020b
RBD	blocks the RBD	EY6A (6ZDH)	GSAS	Y369, F374, S375, T376, F377, K378, C379, Y380, G381, V382, S383, P384, T385, K386, D389, L390, F392, P412, G413, D427, D428, F429, T430	Zhou et al., 2020a

[a]PDB IDs of the cryo-EM structures containing the indicated Ab are given in parentheses.
[b]Epitope residues of SARS-CoV-2 within 4 Å distance of the antibody based on the first PDB ID listed in column 3.

neutralizing mAbs is now increasingly important, with the need to design combination mAbs that target different sites, given the ability of newly emerging variants to potentially evade those Abs that target the RBD site (Andreano et al., 2020; Greaney et al., 2021; Kemp et al., 2020; McCarthy et al., 2020).

We focus here on this polybasic site as a target for mAb binding. In view of the recently detected sequence and structure similarity between the PRRA-insert-enclosing SAg-like motif and the bacterial toxin SEB, we hypothesized that previously generated anti-SEB mAbs might potentially bind the viral SAg-like motif, and in particular the segment $_{682}$RRAR$_{685}$, and might thus block access to the S1/S2 cleavage site. Our *in silico* examination of the possible interactions of known anti-SEB mAbs (Dutta et al., 2015) with SARS-CoV-2 S revealed that SEB-specific mAb 6D3 has a high affinity for binding to the S1/S2 site. Our models further show that the 6D3 binding site overlaps those of TMPRSS2 and/or furin, suggesting that 6D3 might impede viral entry. Experiments conducted with live viruses confirmed that 6D3 inhibited viral entry. Given that its binding site does not overlap those of known Abs (Figure 1C), 6D3 might be used in combination with other neutralizing Abs that target the RBD or other non-overlapping sites to increase efficacy.

RESULTS

Anti-SEB antibody 6D3 is distinguished by its high affinity to bind the SARS-CoV-2 S SAg-like region

As shown in our recent work (Cheng et al., 2020), the S residues E661–R685 that enclose the polybasic segment $_{681}$PRRAR$_{685}$ are sequentially and structurally similar to the segment T150–D161 of SEB. Given this strong similarity, we examined if mAbs specific for SEB (Dutta et al., 2015; Varshney et al., 2011) could neutralize SARS-CoV-2 S. The close proximity (or adjacency) of the SAg-like region to the cleavage bond R685↑S686 further suggested that an anti-SEB mAb that cross-reacts with SARS-CoV-2 would have the added potential to block the cleavage site essential to viral entry, apart from its ability to attenuate the SAg-mediated hyperinflammatory cytokine storm (Krakauer, 2019).

Three SEB-specific mAbs, 14G8, 6D3, and 20B1, have been generated as effective blockers of the SAg activity of SEB in an animal model of TSS (Varshney et al., 2011). Examination of their crystal structures shows that these mAbs bind different sites on SEB (Dutta et al., 2015), as illustrated in Figure 2A. Notably, only 6D3 targets the SEB polybasic segment T150–D161 (shown in dark blue space-filling representation) that is the counterpart of the SARS-CoV-2 S SAg-like motif (Cheng et al., 2020). A close-up view shows the tight interaction between the acidic residues E50, D52, and D55 of the 6D3 heavy chain and four basic residues of SEB (Figure 2B).

As expected, among these three SEB mAbs, 6D3 was the only one able to bind to the SARS-CoV-2 S SAg motif (Figures 2C–2E), consistent with 6D3 binding to the precise SEB fragment that aligns with the spike SAg-like motif. Our computational analysis predicted the 6D3 Ab to bind with an affinity of -14.2 ± 2.3 kcal/mol (see STAR Methods). Notably, acidic residues E50, D52, and D55 from the heavy chain of 6D3 were found to interact with the polybasic insert PRRA in SARS-CoV-2 S, with R682 and R683 playing a central role. Yet, interfacial contacts were quite distributed, involving other SARS-CoV-2 S amino

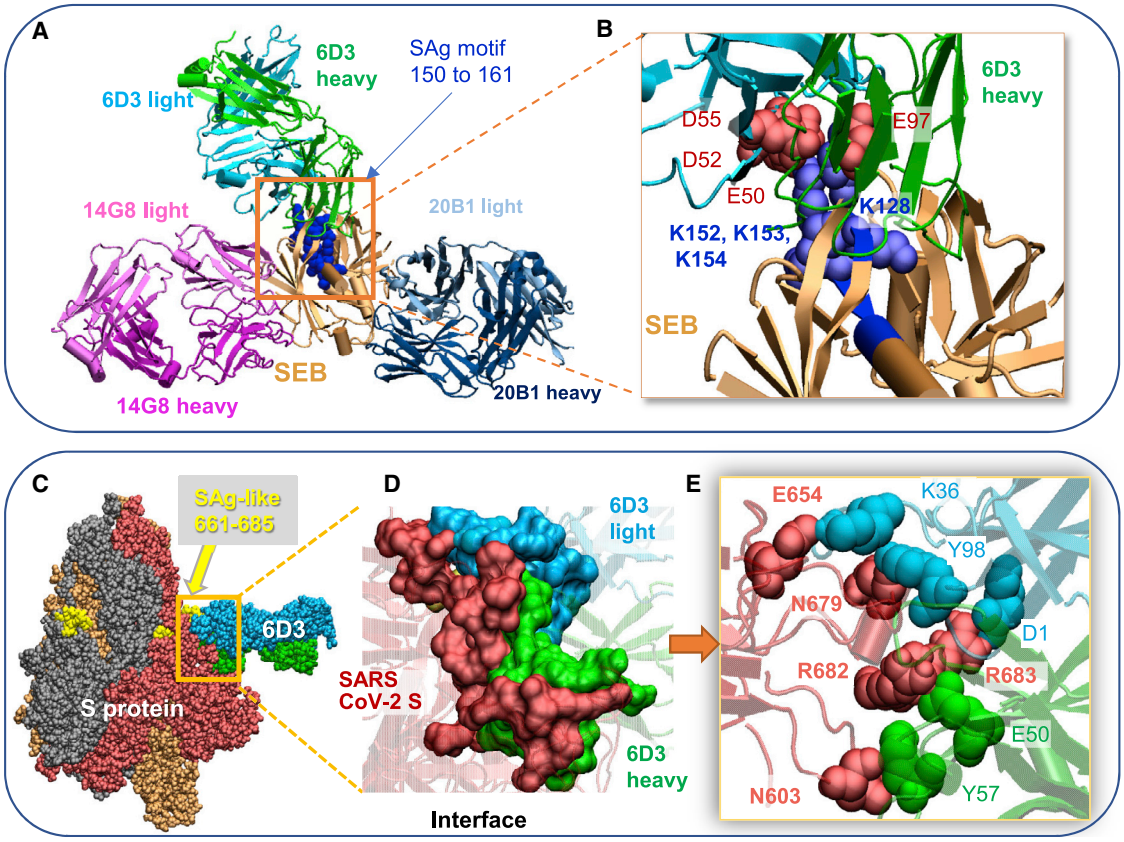

Figure 2. SEB-associated mAb 6D3 binds the furin cleavage site of SARS-CoV-2 S protein, potentially interfering with the S1/S2 cleavage by furin or TMPRSS2

(A and B) Binding pose of three SEB-neutralizing Abs (mAbs 6D3, 14G8, and 20B1) onto SEB. The diagram was generated by superposing the crystal structures (PDB: 4RGN and 4RGM) resolved for the complexes (Dutta et al., 2015). SEB is colored beige, with its SAg motif $_{150}$TNKKKATVQELD$_{161}$ highlighted in blue space-filling. (B) Close-up view of the tight interaction between the acidic residues E50, D52, and D55 of the 6D3 heavy chain and four basic residues of SEB.

(C–E) (C) Interface between 6D3 and SEB SAg motif. Heavy and light chains of 6D3 are green and cyan, respectively. (D) Overall and (E) close-up views of the complex model for S protein and anti-SEB mAb 6D3. The interfacial interactions engage the arginines in the PRRA insert. SARS-CoV-2 S interfacial residues include I210–Q218, N603–Q607, E654–Y660, and A688–I693, and the SAg motif residues Y674, T678–R683. 6D3 interfacial residues include A24–K33, E50, D52, S54, D55, Y57, N59, K74–T77, and A100–A104 in the heavy chain, and D1, I2, Q27, N31–F38, Y55, W56, and D97–Y100 in the light chain. The spike-6D3 complex was generated *in silico* using the S structure modeled with one RBD up (PDB: 6VSB).

acids such as E654, N603, and N679 interacting with either the heavy or the light chain of 6D3 (Figure 2E).

It is interesting to note that among those 6D3-interacting S residues, N603 has been identified as an N-linked glycan site by site-specific glycan analysis of SARS-CoV-2 S (Watanabe et al., 2020) (Figure 3A). To investigate if the glycan sequons might interfere with 6D3 binding, we aligned our spike-6D3 complex model against the glycosylated spike (Woo et al., 2020). No steric overlap was observed between 6D3 and glycan sequons, as illustrated in Figure 3B. Of note is that the N603-linked glycan even assists in the association of 6D3 with the specific binding epitope that overlaps the SAg-like (and S1/S2 cleavage) site, rather than obstructing it. A tight interaction between N603 and Y57 on the 6D3 heavy-chain variable domain (VH) is observed, in addition to potential contacts between the glycan and the 6D3 VH residues Y57–Y60 that further contribute to the stabilization of 6D3 binding. These results indicate that the anti-SEB mAb 6D3 shows high-affinity binding to the SARS-CoV2 SAg-like motif, therefore blocking its interaction with the TCR and potentially attenuating the SAg-mediated T cell activation and cytokine release.

Based on these results, we proposed that 6D3 may decrease the exposure of the cleavage site to the extracellular environment and potentially interfere with SARS-CoV-2 viral entry by competing with the host cell proteases TMPRSS2 and furin, whose binding to the cleavage site is essential to S-protein priming for viral entry. Next, we proceed to the investigation of the potential neutralizing effect of 6D3 tested in live virus experiments.

Anti-SEB antibody, 6D3, inhibits SARS-CoV-2 infection in live virus assays

Here, we investigated whether the SEB-specific mAb 6D3 possessed any neutralizing efficacy *vis-à-vis* SARS-CoV-2 viral entry. To this end, we tested the ability of 6D3 to inhibit SARS-CoV-2 infection in an *in vitro* cell culture infection system. Abs were incubated with SARS-CoV-2 for 1 h and then added to plated Vero-E6 cells. At 48 h post-infection, we analyzed viral infection by immunofluorescence using Abs against double-

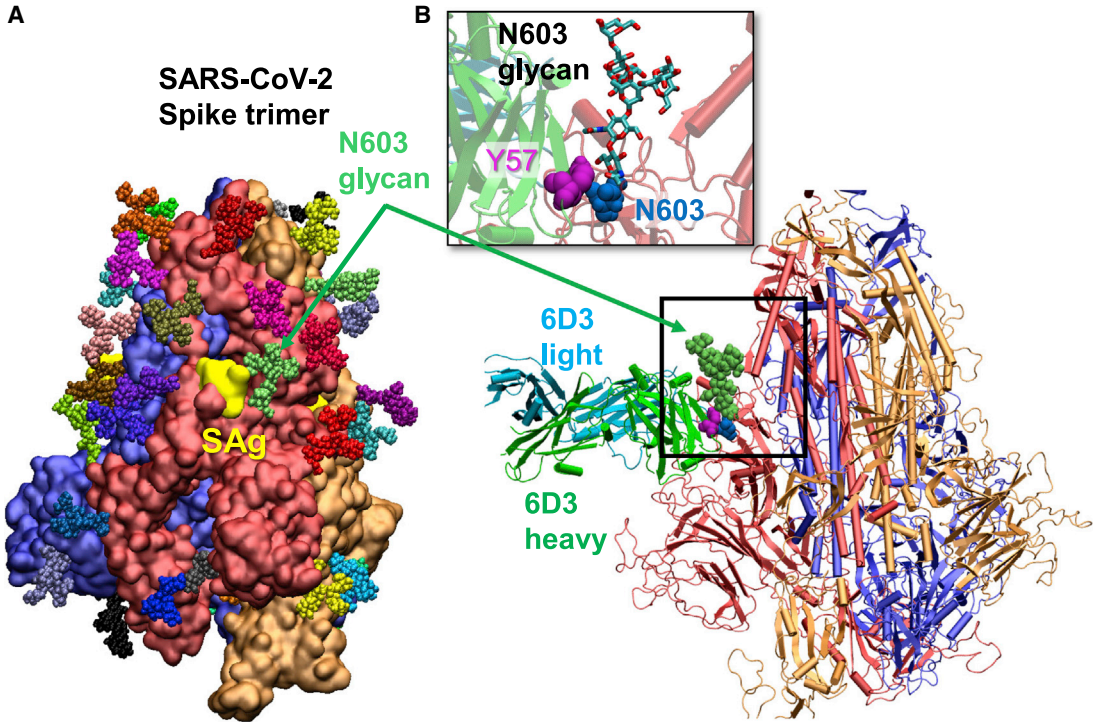

Figure 3. Glycosylation of SARS-CoV-2 spike at N603 does not block mAb 6D3 binding and may even assist in binding the mAb

(A) Computationally modeled SARS-CoV-2 glycosylated spike. The three monomers of the spike protein are shown in blue, red, and orange surface representations, with their SAg region (residues 661–685) colored yellow. High-mannose N-glycans are shown in colored (small) spheres.

(B) Structural alignment of computationally modeled 6D3-spike protein complex onto the glycosylated spike. No spatial clash was observed. The inset shows a close-up view.

stranded RNA (dsRNA) or SARS-CoV-2 S protein (Figures 4 and S1). We found that 6D3 significantly inhibited viral infection, as measured by the percentage of dsRNA-positive cells, at concentrations of 0.8, 4, and 20 μg/mL of Ab, with an IC_{50} of 5.63 μg/mL (Figures 4A, 4B, and S1A). Furthermore, in an independent set of experiments, we found that 6D3 significantly inhibited viral infection, as measured by the percentage of spike-positive cells, at concentrations of 4, 20, and 40 μg/mL of Ab, while there was a trend for inhibition at 0.16 and 0.8 μg/mL of Ab (Figures 4C, 4D, and S1B).

These results indicate that 6D3 can also block viral entry in a concentration-dependent manner, in addition to its high-affinity binding to the SARS-CoV-2 SAg-like motif and potentially blocking its interaction with TCRs. Toward assessing whether 6D3 competitively binds the S1/S2 site in the presence of the proteases, we explored the spike-binding mechanisms and affinities of TMPRSS2 and furin, presented next.

TMPRSS2 and furin bind to the S1/S2 site in close association with the PRRA insert

We analyzed the protease-binding characteristics of the S1/S2 site to assess whether Abs that might target the PRRA site would also hinder the access of proteases. The S1/S2 site, also known as the furin cleavage site, typically contains eight central residues, including the polybasic segment (here $_{680}$SPRRAR↑SV$_{687}$), flanked by solvent-accessible residues on both sides (Tian et al., 2012). The resulting structural models generated for the interactions of TMPRSS2 and furin with the S protein are presented in Figures 5A and 5B, respectively, and more details are reported in Figures S2 and S3. To generate these models, we used the available structural data (Dahms et al., 2016; Walls et al., 2020; Wrapp et al., 2020) for the proteins and the docking software ClusPro (Kozakov et al., 2017) and protocols outlined in the STAR Methods. An ensemble of structural models was generated for each complex, and those conformers satisfying the criteria for S1/S2 cleavage, mainly the positioning of catalytic residues within 3–7 Å atom-atom distance from the cleavage site, were selected for further refinement and energetic evaluation using PRODIGY (Xue et al., 2016).

TMPRSS2 catalytic residues (H296, D345, and S441) were observed to bind near $_{681}$PRRA**RS**$_{686}$ in 7.5% of the generated models (Figure S2B); their binding affinities varied from −14.1 to −11.3 kcal/mol with an average of −12.7 ± 2.0 kcal/mol. Figure 5A displays the most energetically favorable model, in which the three arginines in $_{681}$PRRA**RS**$_{686}$ penetrate the catalytic cavity (Figure 5A, right): R682 forms a salt bridge with TMPRSS2 residue D435, R683 with catalytic aspartate D345, and R685 with TMPRSS2 E299, positioning the scissile bond (spheres) near catalytic residues S441 and H296.

In the case of furin binding, 70% of the structural models showed the catalytic residues (D153, H194, and S368) stabilized in close proximity to $_{681}$PRRA**RS**$_{686}$ (see Figure S3), indicating that binding of furin to the cleavage site was entropically more favorable than that of TMPRSS2. The binding affinities varied

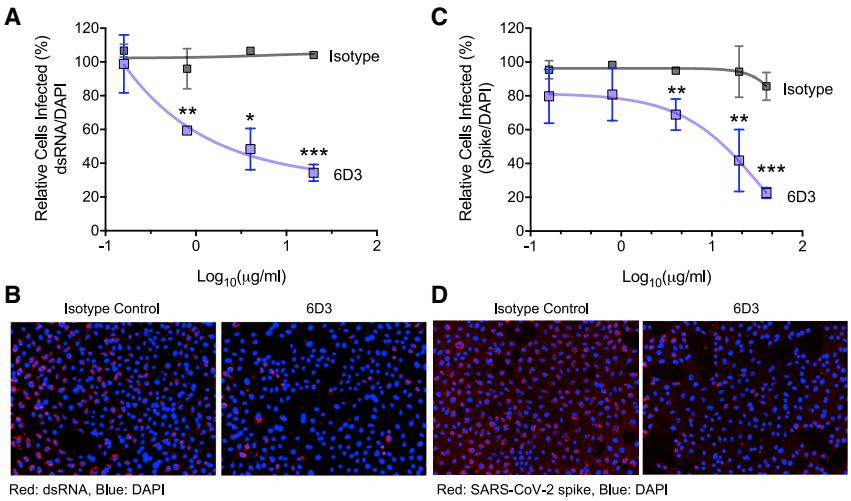

Figure 4. Monoclonal antibody 6D3 prevents SARS-CoV-2 infection

6D3 or isotype control antibodies (at indicated concentrations) were incubated with virus (100 plaque-forming units/well) for 1 h at room temperature before addition to Vero-E6 cells (5×10^3 cells/well). Forty-eight hours post-infection the cells were fixed and stained for dsRNA or SARS-CoV-2 spike protein.

(A) Quantification of the percentage of infected cells per well by dsRNA staining.

(B) Representative fluorescence images of 6D3-mediated inhibition of virus infection (dsRNA).

(C) Quantification of the percentage of infected cells per well by spike staining.

(D) Representative fluorescence images of 6D3-mediated inhibition of virus infection (spike). Data were analyzed by t test (6D3 versus isotype control) with multiple testing correction (false discovery rate). Data are presented as the mean ± standard error of the mean. n = 3 technical replicates. Data are representative of three independent experiments. *$p < 0.05$, **$p < 0.01$, ***$p < 0.001$. See also Figure S1 for detailed results as a function of 6D3 concentration.

from −16.4 to −11.8 kcal/mol with an average of −14.1 ± 2.3 kcal/mol. The best pose with the catalytic residues facing the S1/S2 site, shown in Figures 5B and S3A, reveals the insertion of R682 and R683 into negatively charged pockets of furin to enable the cleavage of the SARS-CoV-2 S.

Overall, our analysis shows that TMPRSS2 or furin engages in tight intermolecular interactions, in which the basic residues R682 and R683 reach out to the catalytic site of either protease. Binding of either enzyme is accommodated by changes in the local conformation near the cleavage region. However, our analysis also suggests that furin binds with higher potency and probability compared with TMPRSS2. Most importantly, 6D3 and the proteases compete for the same binding site (Figure S4). Comparison with the binding affinity of 6D3 evaluated above shows that 6D3 has a spike-binding affinity comparable to that of furin, and stronger than TMPRSS2, suggesting that it can effectively compete with those proteases, in agreement with the experimentally observed efficacy in reducing viral entry.

An acidic residue cluster at VH CDR2 is the hallmark of Abs targeting the furin-like cleavage site

Our study pointed to the distinctive ability of 6D3 to bind to the S1/S2 cleavage site, while other mAbs (in Table 1) did not show such a binding propensity. We investigated which sequence/structure features distinguish 6D3 from others. Abs target viruses mainly through their three complementarity-determining regions (CDR1–CDR3) in the variable domains, especially in the heavy chains (Li et al., 2020). Figure 6A compares the sequences of the VH chains of the SARS-CoV-2 S-associated mAbs and three mAbs associated with SEB. CDR3s exhibit large sequence variation, in accordance with their role in conferring specificity. However, the alignment reveals a unique feature that distinguishes 6D3 and another mAb, 4A8, from all other mAbs: mainly a polyacidic cluster at their CDR2. Specifically, the 6D3 CDR2 possesses three acidic residues, E50, D52, and D55, already noted above to enable binding to the precise cleavage site on the S protein. Likewise, mAb 4A8 has four acidic residues, D52, E54, D55, and D57 (Figure 6A). The mAb 4A8 is known to bind the NTD of the spike (Chi et al., 2020; McCarthy et al., 2020) (Figure S5A). Our docking simulations also indicated that the particular S epitope and 4A8 paratope observed in the cryo-EM structure of the spike-4A8 complex were selected as the most favorable binding pose (Figure S5B). However, the SAg-like motif E661–R685 was also found to be favorable, albeit with a weaker binding affinity (Figure S5C), and could compete with human proteases for binding the same site (Figure S5D). It is interesting to note that our simulations indicated a binding affinity of −13.4 ± 2.4 kcal/mol for the NTD (experimentally observed and computationally most probable) site, consistent with the equilibrium dissociation constant (K_d = 2.14 nM, or corresponding ΔG = −12.3 kcal/mol) measured by biolayer interferometry for the spike-4A8 complex (Chi et al., 2020).

A polyacidic CDR2 at the VH chain thus emerges as a hallmark of the mAbs that target the polybasic furin-like cleavage site. As shown in Figure 6B, these acidic residues facilitate Ab-spike complexation through salt bridges formed with the basic residues (R682, R683, and R685) in $_{680}$SPRRARSV$_{687}$, the central component of typical furin cleavage sites (Tian et al., 2012), thus attenuating, if not blocking, access of proteases.

As shown in Figure 1B, the polybasic insertion of SARS-CoV-2 is not shared by other SARS-family βCoVs, but is found in common cold HCoVs HKU1 and OC43, and in MERS. The present findings strongly suggest that mAb 6D3 may also target these other HCoVs that encode a furin cleavage site. We investigated the binding properties of 6D3 to a structural model for HCoV-OC43 S based on the OC43 S cryo-EM structure (PDB: 6NZK) (Tortorici et al., 2019). The highest-affinity binding pose predicted by our simulations is presented in Figure 6C, suggesting that 6D3 binds the S1/S2 cleavage site of HCoV-OC43 S. Again, polyacidic residues in CDR2 play a primary role in binding to the cleavage site of HCoV-OC43 S. These findings highlight the potential effectiveness and cross-reactivity of 6D3 targeting the furin cleavage site between the S protein of SARS-CoV-2 and other selected HCoVs.

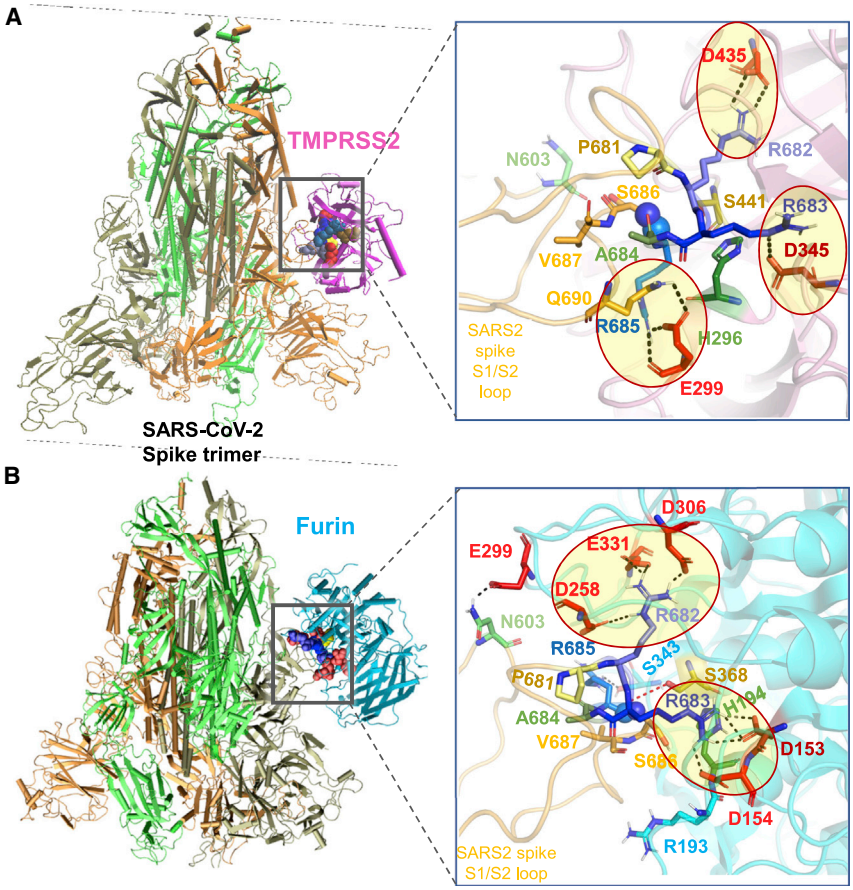

Figure 5. Binding poses of human proteases TMPRSS2 and furin to SARS-CoV-2 S protein

(A and B) Structural models for the SARS-CoV-2 S protein complexed with (A) TMPRSS2 and (B) furin, obtained from docking simulations followed by refinements. An overview (left) and a zoomed-in view (right) are shown in each case. The arginines in the S1/S2 loop $P_{681}RRARS_{686}$ are shown in different shades of blue, and their interaction partners (acidic residues) in the proteases are shown in red. Spheres (right) highlight the R685↑S686 peptide bond. The TMPRSS2 catalytic triad residues are S441 (yellow), H296 (green), and D345 (dark red). Their counterparts in furin are S368, H194, and D153. Note the short distance between the carbonyl carbon of R685 and the hydroxyl oxygen of S441 of TMPRSS2 (3.5 Å) or S368 of furin (3.1 Å). Black dashed lines show interfacial polar contacts and salt bridges, and those including the S1/S2 loop arginines are highlighted by ellipses.

DISCUSSION

A new strategy for combatting SARS-CoV-2: repurposing of antibodies that target the S1/S2 cleavage site

SARS-CoV-2 S is the main determinant of cell entry and the major target of neutralizing Abs (Cao et al., 2020b; Chi et al., 2020; Hansen et al., 2020; Pinto et al., 2020; Renn et al., 2020; Shi et al., 2020; Yuan et al., 2020). The majority of COVID-19 Ab therapies under investigation are designed to target the S protein RBD, while other potential neutralizing epitopes have also been found (Cao et al., 2020b; Chi et al., 2020; Hansen et al., 2020; Liu et al., 2020; Pinto et al., 2020; Renn et al., 2020; Shi et al., 2020; Yuan et al., 2020). Given the high glycosylation and antigenic variability of SARS-CoV-2 S (Graham et al., 2019), a combination of mAbs that target multiple sites and multiple conformations of SARS-CoV-2 S is likely the most effective strategy. In addition to blocking ACE2 binding, distinct neutralizing mechanisms have been proposed, including Ab-dependent cell cytotoxicity and phagocytosis (Pinto et al., 2020) and restraining the structural changes of SARS-CoV-2 spike (Chi et al., 2020).

Proteolytic cleavage of SARS-CoV-2 S is the second critical step, succeeding ACE2 binding, in the life cycle of SARS-CoV-2. TMPRSS2 and furin inhibitors have been found to block the cell entry of SARS-CoV-2 (Bestle et al., 2020; Hoffmann et al., 2020). The critical role of the furin cleavage site in SARS-CoV-2 infectivity and Ab activity is also demonstrated in a recent study where the deletion ΔPRRA reduced SARS-CoV-2 viral replication in a human respiratory cell line and attenuated infectivity (Johnson et al., 2021). Unlike TMPRSS2, furin is a ubiquitous proprotein convertase and is required for normal development and function (Thomas, 2002), and its inhibition is not a viable strategy. But, the design or repurposing of Abs that block the S1/S2 site is an attractive alternative solution that avoids effects on the (other) activities of TMPRSS2 and furin.

It is well known that the SARS-CoV-2 spike is heavily glycosylated, and the possible interference of glycans with Ab binding is a plausible consideration (Casalino et al., 2020). Notably, 6D3 binding did not give rise to a steric clash with the N-linked glycan sequons near the S1/S2 site (e.g., N603 or N657/N658 as reported; Watanabe et al., 2020). In addition, SARS-CoV-2 S was predicted to be O-glycosylated at S673, T678, and S686 near the S1/S2 cleavage site (Andersen et al., 2020), yet to be confirmed by experiments (Shajahan et al., 2020; Watanabe et al., 2020). Therefore, 6D3 is expected to target directly the S1/S2 site of SARS-CoV-2 S (as the host proteases do) without any shielding effect by glycans. In contrast, the glycosylation near N603 may even assist in promoting its binding near the PRRA site. Interestingly, the possible modulating role of glycans on the structure and dynamics of the S glycoprotein has been pointed out to be a feature that could be harnessed in anti-SARS-CoV-2 vaccine development (Casalino et al., 2020).

The ability of the polybasic insert to bind antibodies may have escaped prior cryo-EM studies with mutant S protein

It has been a challenge to resolve the S1/S2 loop in cryo-EM studies of HCoV S proteins. First, pre-activation of HCoV S during protein preparation results in a mixture of cleaved and

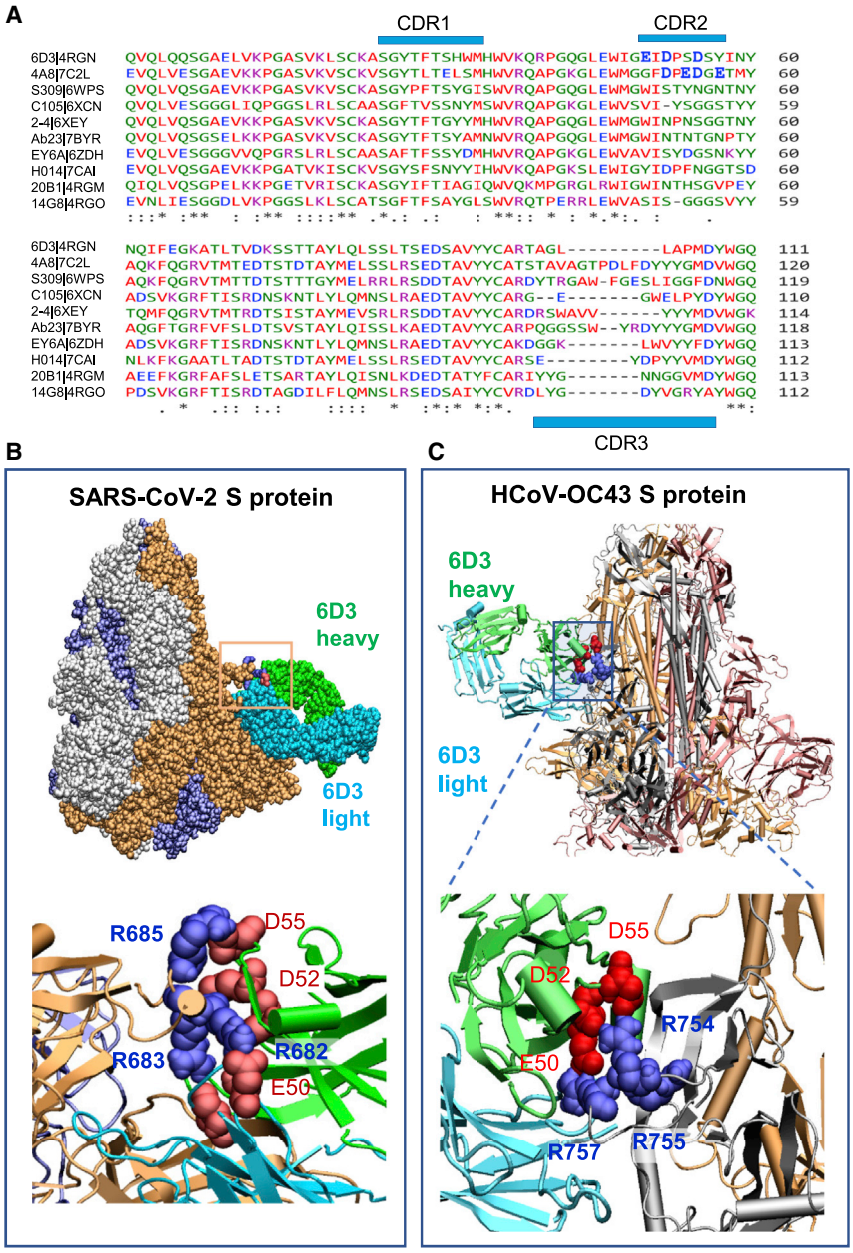

Figure 6. Polyacidic residues in CDR2 of the mAbs 6D3 heavy chain play a major role in blocking the furin-like cleavage site of SARS-CoV-2 S protein

(A) Multiple sequence alignment of the VH domain of anti-SEB Abs (6D3, 14G8, and 20B1) and anti-SARS-CoV-2 S Abs (see the names on the left). The residue ranges of the three CDRs are CDR1, residues 25 to 32; CDR2, 51 to 58; and CDR3, 100 to 116 (Chi et al., 2020), as indicated by the blue bars.

(B) Overall and close-up views of the complex and interfacial interaction of the spike protein complexed with 6D3 antibody. Note that three acidic residues from CDR2 interact with the basic residues R682, R683, and R685 of the S protein. The complex was generated *in silico* using the SARS-CoV-2 S structure with all three RBDs in the down conformer (PDB: 6VXX).

(C) Same as (B), repeated for the human cold virus HCoV-OC43 S protein. The complex was generated *in silico* using the HCoV-OC43 S structure with all three RBDs in the down conformer (PDB: 6NZK). HCoV-OC43 encodes an S1/S2 furin-like cleavage site at $_{754}$RRAR↑G$_{758}$. Note that three acidic residues from CDR2 interact with R754, R755, and R757 in HCoV-OC43 S protein. The residues belonging to the Abs are labeled in regular font and those of the S protein in bold in both (B) and (C).

uncleaved spikes (Cai et al., 2020). Second, local conformational changes near the S1/S2 region may differ between cleaved and intact structures, as observed in influenza viruses (Steinhauer, 1999). Third, multiple conformations, if not a disordered state, may exist near that region, as indicated by microsecond simulations and *ab initio* modeling (Lemmin et al., 2020). Therefore, most cryo-EM studies of SARS-CoV-2 S protein complexed with Abs have resorted to variants where the $_{682}$RRAR$_{685}$ segment has been replaced by GSAS or SGAG (Barnes et al., 2020; Cao et al., 2020b; Chi et al., 2020; Liu et al., 2020; Lv et al., 2020b; Pinto et al., 2020; Zhou et al., 2020a; Zost et al., 2020) (Table 1). These "mutant spikes" may have precluded the discovery of the binding of Abs to the S1/S2 site. Molecular modeling and simulations provided insights into the interactions at this region, including those with proteases and other receptors (Cheng et al., 2020; Jaimes et al., 2020; Lemmin et al., 2020). We undertook such modeling studies (Figures 2C–2E, 3, 5, and 6) and performed live-virus experiments (Figures 4 and S1) to investigate the Abs that possibly interfere with the binding of TMPRSS2 and furin. To our knowledge, we identified an Ab (6D3) that may block the S1/S2 cleavage site in SARS-CoV-2 S protein. We note that, due to the conformational variability of the S1/S2 loop, the actual binding site of 6D3 on SARS-CoV-2 S may be different from that predicted by computational models, and there may be multiple binding sites on S, as predicted for the Ab 4A8 (Figure S5). The precise binding site and pose of 6D3 will need to be resolved by structural studies.

6D3 is a repurposable anti-SEB mAb that targets the S1/S2 site and inhibits viral infection

6D3 is an Ab originally discovered for neutralizing the superantigenic bacterial toxin SEB. Here we are proposing its use as a repurposable mAb against SARS-CoV-2 S protein, by virtue of its ability to bind a sequence motif shared between SEB and S protein. Our recent study revealed the high similarity between SARS-CoV-2 S amino acids E661–R685 and SEB amino acids T150–D161, which may contribute to hyperinflammation and MIS-C/A pathogenesis through a SAg-induced immune activation (Cheng et al., 2020). This hypothesis was supported by the

clinical and laboratory features observed in MIS-C and severe COVID-19 patients, which were similar to those of TSS caused by bacterial toxins such as SEB (Cheng et al., 2020; Noval Rivas et al., 2020). Adult patients with severe COVID-19 (Cheng et al., 2020), as well as children with MIS-C (Porritt et al., 2020), displayed TCR skewing typical of SAg-induced immune responses. Among the three mAbs discovered against SEB, 6D3 was the only one specific to the region of interest (Figures 2A and 2B), and computations and experiments corroborated our hypothesis that this anti-SEB mAb could bind to the SARS-CoV-2 S protein.

Another feature that caught our attention was the fact that this SAg-like segment (that binds 6D3) overlapped with the furin-like cleavage site characteristic of SARS-CoV-2 (and MERS and the HCoVs HKU1 and OC43; see Figure 1B). Furin cleavage sites usually involve ~20 residues, 8 of which play a central role (Tian et al., 2012). In the case of SARS-CoV-2, the segment $_{680}$SPRRAR↑SV$_{687}$ of the S protein forms this central component. Simulations indeed showed strong interactions (salt bridges) formed between 6D3 VH CDR2 (distinguished by a stretch of acidic residues) and the polybasic $_{682}$RRAR$_{685}$ (Figures 2C–2E and 6B), and *in vitro* assays confirmed that 6D3 inhibited viral entry (Figures 4 and S1).

By binding the viral spike protein, SARS-CoV-2-specific Abs in the blood or mucosal surface could prevent the virus from binding to and infecting target cells. The Ab neutralization assay that we performed in cell culture simulates this scenario, where the specific mAb 6D3 incubated with SARS-CoV-2 binds and neutralizes the virus's ability to attach to the cell receptor and to initiate infection *in vitro*. Thus, mAb 6D3 may have a differentiating dual role in not only inhibiting viral entry but also potentially blocking the SARS-CoV-2 SAg-like motif-induced T cell activation, cytokine storm, and hyperinflammation. The next experimental steps assessing the *in vivo* effect of mAb 6D3 in relevant mouse models of SARS-CoV-2 infection are currently underway.

mAbs with a cluster of acidic residues at their VH CDR2 may mitigate viral infections caused by CoVs that contain furin-like cleavage sites

HCoVs include three highly pathogenic viruses, SARS-CoV-2, SARS-CoV, and MERS, and four circulating endemic viruses (HCoV-NL63, HCoV-229E, HCoV-OC43, and HKU1), which cause mild to moderate upper respiratory diseases (Coutard et al., 2020; Cui et al., 2019; Forni et al., 2017). Interestingly, many individuals who have not been exposed to SARS-CoV-2 possess SARS-CoV-2 spike-reactive T cells, due to cross-reaction of immune responses generated against other HCoV strains (Grifoni et al., 2020; Mateus et al., 2020). Cross-reactive Abs between human βCoV strains have also been identified, including those between SARS and SARS-CoV-2 (Huang et al., 2020; Lv et al., 2020a). Indeed, SARS mAb S309 can potently neutralize both SARS and SARS-CoV-2 (Pinto et al., 2020). Furthermore, the effectiveness of intravenous immunoglobulin (Belhadjer et al., 2020; Riphagen et al., 2020; Verdoni et al., 2020) may, in part, be due to the presence of cross-reactive Abs against other HCoV strains. These findings raise the exciting possibility of designing wide-spectrum Abs with cross-reactivity among HCoVs. The two Abs (6D3 and 4A8) identified in this study to present the suitable paratope for binding the PRRAR or similar polybasic inserts may potentially block the S1/S2 cleavage site in HCoVs that encode furin-like cleavage sites (Figure 6), providing additional benefit beyond those applicable to the current pandemic. The hallmark polyacidic residues in the CDR2 of VH may be exploited as a benchmark to sort out mAbs that can potentially target the SARS-CoV-2 furin cleavage site.

Alternative strategies targeting the S1/S2 site in light of these repurposable mAbs

Based on the scaffold of the 6D3 heavy chain, mini-proteins may be designed to target SARS-CoV-2, MERS, HCoV-OC43, or HKU1, to block CoV entry. Notably, designed *de novo* mini-proteins have been shown to block ACE2 binding, based on the scaffold of ACE2 (Cao et al., 2020a). Very recently, neuropilin-1 (NRP1) has been identified as a host factor for SARS-CoV-2 infection, bound to the $_{681}$RRAR$_{685}$ segment (Daly et al., 2020). Remarkably, blockade of this interaction by RNAi or mAb against NRP1 significantly reduced *in vitro* SARS-CoV-2 cellular entry (Cantuti-Castelvetri et al., 2020; Daly et al., 2020). We anticipate that 6D3 may block the binding of NRP1. At present, no clinical treatments or prevention strategies are available for HCoVs (Cui et al., 2019). Our work may lead to an improved understanding of coronavirus immunity, facilitating future studies to understand the mechanisms of Ab recognition and neutralization and help screen SARS-CoV-2 Abs for treatment of COVID-19. These findings also raise exciting possibilities of designing therapeutic approaches using a combination of 6D3 and known neutralizing mAbs that bind the RBD, for possibly treating severe COVID-19 and MIS-C/A patients and/or combatting the spread of the newly emerging variants.

STAR★METHODS

Detailed methods are provided in the online version of this paper and include the following:

- KEY RESOURCES TABLE
- RESOURCE AVAILABILITY
  - Lead contact
  - Materials availability
  - Data and code availability
- EXPERIMENTAL MODEL AND SUBJECT DETAILS
- METHOD DETAILS
  - *In vitro* viral inhibition assays
  - Structural data for SARS-CoV-2, human TMPRSS2 and furin
  - Generation and assessment of SARS-CoV-2 Spike and protease complex models
  - Monoclonal antibodies binding to SARS-CoV-2 Spike
  - Model refinement and binding affinity calculations
  - Sequence alignment
- QUANTIFICATION AND STATISTICAL ANALYSIS
  - For viral inhibition assays

SUPPLEMENTAL INFORMATION

Supplemental information can be found online at https://doi.org/10.1016/j.str.2021.04.005.

ACKNOWLEDGMENTS

We gratefully acknowledge support from NIH awards 3RO1AI072726-10S1 (to M.A.) and P41GM103712 (to I.B.) and a MolSSI COVID-19 Seed Software Fellowship (to J.K.). This study was in part funded with resources provided by US Veterans Affairs Merit Review Award 5I01 BX003741 (to B.C.F.). B.C.F. is an attending physician at the US Department of Veterans Affairs-Northport VA Medical Center, Northport, NY. The contents of this study do not represent the views of the VA or the US government.

AUTHOR CONTRIBUTIONS

M.H.C., I.B., and M.A. designed and supervised the work. M.H.C. did the computations, assisted by J.K. I.B. and M.H.C. analyzed the computational results. V.A. and G.G. performed the *in vitro* viral infections. A.B.O. and R.A.P. analyzed the experimental *in vitro* data. B.C.F. provided purified mAb and interpreted experimental data. M.H.C., R.A.P., M.N.R., M.A., and I.B. wrote the manuscript.

DECLARATION OF INTERESTS

The authors declare no competing interests.

Received: January 29, 2021
Revised: February 28, 2021
Accepted: April 8, 2021
Published: April 29, 2021

REFERENCES

Andersen, K.G., Rambaut, A., Lipkin, W.I., Holmes, E.C., and Garry, R.F. (2020). The proximal origin of SARS-CoV-2. Nat. Med. *26*, 450–452.

Andreano, E., Piccini, G., Licastro, D., Casalino, L., Johnson, N.V., Paciello, I., Monego, S.D., Pantano, E., Manganaro, N., Manenti, A., et al. (2020). SARS-CoV-2 escape in vitro from a highly neutralizing COVID-19 convalescent plasma. bioRxiv. https://doi.org/10.1101/2020.12.28.424451.

Barnes, C.O., West, A.P., Huey-Tubman, K., Hoffmann, M.A., Sharaf, N.G., Hoffman, P.R., Koranda, N., Gristick, H.B., Gaebler, C., and Muecksch, F. (2020). Structures of human antibodies bound to SARS-CoV-2 spike reveal common epitopes and recurrent features of antibodies. Cell *182*, 828–842.

Belhadjer, Z., Méot, M., Bajolle, F., Khraiche, D., Legendre, A., Abakka, S., Auriau, J., Grimaud, M., Oualha, M., Beghetti, M., et al. (2020). Acute heart failure in multisystem inflammatory syndrome in children (MIS-C) in the context of global SARS-CoV-2 pandemic. Circulation *142*, 429–436.

Benton, D.J., Wrobel, A.G., Xu, P., Roustan, C., Martin, S.R., Rosenthal, P.B., Skehel, J.J., and Gamblin, S.J. (2020). Receptor binding and priming of the spike protein of SARS-CoV-2 for membrane fusion. Nature *588*, 327–330.

Bestle, D., Heindl, M.R., Limburg, H., Van Lam van, T., Pilgram, O., Moulton, H., Stein, D.A., Hardes, K., Eickmann, M., Dolnik, O., et al. (2020). TMPRSS2 and furin are both essential for proteolytic activation of SARS-CoV-2 in human airway cells. Life Sci. Alliance *3*, e202000786.

Cai, Y., Zhang, J., Xiao, T., Peng, H., Sterling, S.M., Walsh, R.M., Jr., Rawson, S., Rits-Volloch, S., and Chen, B. (2020). Distinct conformational states of SARS-CoV-2 spike protein. Science *369*, 1586–1592.

Cantuti-Castelvetri, L., Ojha, R., Pedro, L.D., Djannatian, M., Franz, J., Kuivanen, S., van der Meer, F., Kallio, K., Kaya, T., and Anastasina, M. (2020). Neuropilin-1 facilitates SARS-CoV-2 cell entry and infectivity. Science *370*, 856–860.

Cao, L., Goreshnik, I., Coventry, B., Case, J.B., Miller, L., Kozodoy, L., Chen, R.E., Carter, L., Walls, A.C., Park, Y.-J., et al. (2020a). De novo design of picomolar SARS-CoV-2 miniprotein inhibitors. Science *370*, 426–431.

Cao, Y., Su, B., Guo, X., Sun, W., Deng, Y., Bao, L., Zhu, Q., Zhang, X., Zheng, Y., Geng, C., et al. (2020b). Potent neutralizing antibodies against SARS-CoV-2 identified by high-throughput single-cell sequencing of convalescent patients' B cells. Cell *182*, 73–84.e16.

Casalino, L., Gaieb, Z., Goldsmith, J.A., Hjorth, C.K., Dommer, A.C., Harbison, A.M., Fogarty, C.A., Barros, E.P., Taylor, B.C., McLellan, J.S., et al. (2020). Beyond shielding: the roles of glycans in the SARS-CoV-2 Spike protein. ACS Cent. Sci. *6*, 1722–1734.

Cheng, M.H., Zhang, S., Porritt, R.A., Arditi, M., and Bahar, I. (2020). Superantigenic character of an insert unique to SARS-CoV-2 spike supported by skewed TCR repertoire in patients with hyperinflammation. Proc. Natl. Acad. Sci. U S A *117*, 25254–25262.

Cheung, E.W., Zachariah, P., Gorelik, M., Boneparth, A., Kernie, S.G., Orange, J.S., and Milner, J.D. (2020). Multisystem inflammatory syndrome related to COVID-19 in previously healthy children and adolescents in New York city. JAMA *324*, 294–296.

Chi, X., Yan, R., Zhang, J., Zhang, G., Zhang, Y., Hao, M., Zhang, Z., Fan, P., Dong, Y., Yang, Y., et al. (2020). A neutralizing human antibody binds to the N-terminal domain of the Spike protein of SARS-CoV-2. Science *369*, 650–655.

Coutard, B., Valle, C., de Lamballerie, X., Canard, B., Seidah, N.G., and Decroly, E. (2020). The spike glycoprotein of the new coronavirus 2019-nCoV contains a furin-like cleavage site absent in CoV of the same clade. Antivir. Res. *176*, 104742.

Cui, J., Li, F., and Shi, Z.-L. (2019). Origin and evolution of pathogenic coronaviruses. Nat. Rev. Microbiol. *17*, 181–192.

Dahms, S.O., Creemers, J.W., Schaub, Y., Bourenkov, G.P., Zogg, T., Brandstetter, H., and Than, M.E. (2016). The structure of a furin-antibody complex explains non-competitive inhibition by steric exclusion of substrate conformers. Sci. Rep. *6*, 34303.

Daly, J.L., Simonetti, B., Klein, K., Chen, K.-E., Williamson, M.K., Antón-Plágaro, C., Shoemark, D.K., Simón-Gracia, L., Bauer, M., Hollandi, R., et al. (2020). Neuropilin-1 is a host factor for SARS-CoV-2 infection. Science *370*, 861–865.

DeLano, W.L. (2002). Pymol: an open-source molecular graphics tool. CCP4 Newsl. Protein Crystallogr. *40*, 82–92.

Dutta, K., Varshney, A.K., Franklin, M.C., Goger, M., Wang, X., and Fries, B.C. (2015). Mechanisms mediating enhanced neutralization efficacy of staphylococcal enterotoxin B by combinations of monoclonal antibodies. J. Biol. Chem. *290*, 6715–6730.

Forni, D., Cagliani, R., Clerici, M., and Sironi, M. (2017). Molecular evolution of human coronavirus genomes. Trends Microbiol. *25*, 35–48.

Garcia, G., Sharma, A., Ramaiah, A., Sen, C., Kohn, D., Gomperts, B., Svendsen, C.N., Damoiseaux, R.D., and Arumugaswami, V. (2020). Antiviral drug screen of kinase inhibitors identifies cellular signaling pathways critical for SARS-CoV-2 replication. bioRxiv. https://doi.org/10.1101/2020.06.24.150326.

Graham, B.S., Gilman, M.S.A., and McLellan, J.S. (2019). Structure-based vaccine antigen design. Annu. Rev. Med. *70*, 91–104.

Greaney, A.J., Starr, T.N., Gilchuk, P., Zost, S.J., Binshtein, E., Loes, A.N., Hilton, S.K., Huddleston, J., Eguia, R., Crawford, K.H.D., et al. (2021). Complete mapping of mutations to the SARS-CoV-2 spike receptor-binding domain that escape antibody recognition. Cell Host Microbe *29*, 44–57.e49.

Grifoni, A., Weiskopf, D., Ramirez, S.I., Mateus, J., Dan, J.M., Moderbacher, C.R., Rawlings, S.A., Sutherland, A., Premkumar, L., Jadi, R.S., et al. (2020). Targets of T cell responses to SARS-CoV-2 coronavirus in humans with COVID-19 disease and unexposed individuals. Cell *181*, 1489–1501 e1415.

Gupta, A., Madhavan, M.V., Sehgal, K., Nair, N., Mahajan, S., Sehrawat, T.S., Bikdeli, B., Ahluwalia, N., Ausiello, J.C., Wan, E.Y., et al. (2020). Extrapulmonary manifestations of COVID-19. Nat. Med. *26*, 1017–1032.

Hansen, J., Baum, A., Pascal, K.E., Russo, V., Giordano, S., Wloga, E., Fulton, B.O., Yan, Y., Koon, K., Patel, K., et al. (2020). Studies in humanized mice and convalescent humans yield a SARS-CoV-2 antibody cocktail. Science *369*, 1010–1014.

Hoffmann, M., Kleine-Weber, H., Schroeder, S., Krüger, N., Herrler, T., Erichsen, S., Schiergens, T.S., Herrler, G., Wu, N.-H., Nitsche, A., et al. (2020). SARS-CoV-2 cell entry depends on ACE2 and TMPRSS2 and is blocked by a clinically proven protease inhibitor. Cell *181*, 271–280.

Huang, A.T., Garcia-Carreras, B., Hitchings, M.D.T., Yang, B., Katzelnick, L.C., Rattigan, S.M., Borgert, B.A., Moreno, C.A., Solomon, B.D., Trimmer-Smith, L., et al. (2020). A systematic review of antibody mediated immunity to coronaviruses: kinetics, correlates of protection, and association with severity. Nat. Commun. *11*, 4704.

Jaimes, J.A., André, N.M., Chappie, J.S., Millet, J.K., and Whittaker, G.R. (2020). Phylogenetic analysis and structural modeling of SARS-CoV-2 spike protein reveals an evolutionary distinct and proteolytically sensitive activation loop. J. Mol. Biol. *432*, 3309–3325.

Johnson, B.A., Xie, X., Bailey, A.L., Kalveram, B., Lokugamage, K.G., Muruato, A., Zou, J., Zhang, X., Juelich, T., Smith, J.K., et al. (2021). Loss of furin cleavage site attenuates SARS-CoV-2 pathogenesis. Nature *591*, 293–299.

Kemp, S., Collier, D., Datir, R., Gayed, S., Jahun, A., Hosmillo, M., Ferreira, I., Rees-Spear, C., Mlcochova, P., Lumb, I.U., et al. (2020). Neutralising antibodies drive spike mediated SARS-CoV-2 evasion. medRxiv. https://doi.org/10.1101/2020.12.05.20241927.

Kozakov, D., Hall, D.R., Xia, B., Porter, K.A., Padhorny, D., Yueh, C., Beglov, D., and Vajda, S. (2017). The ClusPro web server for protein–protein docking. Nat. Protoc. *12*, 255.

Krakauer, T. (2019). Staphylococcal superantigens: pyrogenic toxins induce toxic shock. Toxins *11*, 178.

Lemmin, T., Kalbermatter, D., Harder, D., Plattet, P., and Fotiadis, D. (2020). Structures and dynamics of the novel S1/S2 protease cleavage site loop of the SARS-CoV-2 spike glycoprotein. J. Struct. Biol. X *4*, 100038.

Li, W., Schäfer, A., Kulkarni, S.S., Liu, X., Martinez, D.R., Chen, C., Sun, Z., Leist, S.R., Drelich, A., Zhang, L., et al. (2020). High potency of a bivalent human VH domain in SARS-CoV-2 animal models. Cell *183*, 429–441.e16.

Liu, L., Wang, P., Nair, M.S., Yu, J., Rapp, M., Wang, Q., Luo, Y., Chan, J.F., Sahi, V., Figueroa, A., et al. (2020). Potent neutralizing antibodies directed to multiple epitopes on SARS-CoV-2 spike. Nature *584*, 450–456.

Lv, H., Wu, N.C., Tsang, O.T., Yuan, M., Perera, R., Leung, W.S., So, R.T.Y., Chan, J.M.C., Yip, G.K., Chik, T.S.H., et al. (2020a). Cross-reactive antibody response between SARS-CoV-2 and SARS-CoV infections. Cell Rep. *31*, 107725.

Lv, Z., Deng, Y.-Q., Ye, Q., Cao, L., Sun, C.-Y., Fan, C., Huang, W., Sun, S., Sun, Y., Zhu, L., et al. (2020b). Structural basis for neutralization of SARS-CoV-2 and SARS-CoV by a potent therapeutic antibody. Science *369*, 1505–1509.

Mateus, J., Grifoni, A., Tarke, A., Sidney, J., Ramirez, S.I., Dan, J.M., Burger, Z.C., Rawlings, S.A., Smith, D.M., Phillips, E., et al. (2020). Selective and cross-reactive SARS-CoV-2 T cell epitopes in unexposed humans. Science *370*, 89–94.

Matsuyama, S., Nao, N., Shirato, K., Kawase, M., Saito, S., Takayama, I., Nagata, N., Sekizuka, T., Katoh, H., Kato, F., et al. (2020). Enhanced isolation of SARS-CoV-2 by TMPRSS2-expressing cells. Proc. Natl. Acad. Sci. U S A *117*, 7001–7003.

McCarthy, K.R., Rennick, L.J., Nambulli, S., Robinson-McCarthy, L.R., Bain, W.G., Haidar, G., and Duprex, W.P. (2020). Natural deletions in the SARS-CoV-2 spike glycoprotein drive antibody escape. bioRxiv. https://doi.org/10.1101/2020.11.19.389916.

Noval Rivas, M., Porritt, R.A., Cheng, M.H., Bahar, I., and Arditi, M. (2020). COVID-19-associated multisystem inflammatory syndrome in children (MIS-C): a novel disease that mimics toxic shock syndrome-the superantigen hypothesis. J. Allergy Clin. Immunol. 31414–31417.

Peitsch, M.C. (1995). Protein modeling by E-mail. Bio/Technol. *13*, 658–660.

Pinto, D., Park, Y.-J., Beltramello, M., Walls, A.C., Tortorici, M.A., Bianchi, S., Jaconi, S., Culap, K., Zatta, F., De Marco, A., et al. (2020). Cross-neutralization of SARS-CoV-2 by a human monoclonal SARS-CoV antibody. Nature *583*, 290–295.

Porritt, R.A., Paschold, L., Rivas, M.N., Cheng, M.H., Yonker, L.M., Chandnani, H., Lopez, M., Simnica, D., Schultheiß, C., Santiskulvong, C., et al. (2020). HLA class I-associated expansion of TRBV11-2 T cells via a CDR3-independent mechanism in multisystem inflammatory syndrome in children (MIS-C). J. Clin. Invest. 146614, https://doi.org/10.1172/JCI146614.

Renn, A., Fu, Y., Hu, X., Hall, M.D., and Simeonov, A. (2020). Fruitful neutralizing antibody pipeline brings hope to defeat SARS-Cov-2. Trends Pharmacol. Sci. *41*, 815–829.

Riphagen, S., Gomez, X., Gonzalez-Martinez, C., Wilkinson, N., and Theocharis, P. (2020). Hyperinflammatory shock in children during COVID-19 pandemic. Lancet *395*, 1607–1608.

Shajahan, A., Supekar, N.T., Gleinich, A.S., and Azadi, P. (2020). Deducing the N- and O-glycosylation profile of the spike protein of novel coronavirus SARS-CoV-2. Glycobiology *30*, 981–988.

Shang, J., Wan, Y., Luo, C., Ye, G., Geng, Q., Auerbach, A., and Li, F. (2020). Cell entry mechanisms of SARS-CoV-2. Proc. Natl. Acad. Sci. U S A *117*, 11727–11734.

Shi, R., Shan, C., Duan, X., Chen, Z., Liu, P., Song, J., Song, T., Bi, X., Han, C., Wu, L., et al. (2020). A human neutralizing antibody targets the receptor-binding site of SARS-CoV-2. Nature *584*, 120–124.

Sievers, F., Wilm, A., Dineen, D., Gibson, T.J., Karplus, K., Li, W., Lopez, R., McWilliam, H., Remmert, M., Söding, J., et al. (2011). Fast, scalable generation of high-quality protein multiple sequence alignments using Clustal Omega. Mol. Syst. Biol. *7*, 539.

Steinhauer, D.A. (1999). Role of hemagglutinin cleavage for the pathogenicity of influenza virus. Virology *258*, 1–20.

Tay, M.Z., Poh, C.M., Rénia, L., MacAry, P.A., and Ng, L.F.P. (2020). The trinity of COVID-19: immunity, inflammation and intervention. Nat. Rev. Immunol. *20*, 363–374.

Thomas, G. (2002). Furin at the cutting edge: from protein traffic to embryogenesis and disease. Nat. Rev. Mol. Cell Biol. *3*, 753–766.

Tian, S., Huajun, W., and Wu, J. (2012). Computational prediction of furin cleavage sites by a hybrid method and understanding mechanism underlying diseases. Sci. Rep. *2*, 261.

Tortorici, M.A., Walls, A.C., Lang, Y., Wang, C., Li, Z., Koerhuis, D., Boons, G.J., Bosch, B.J., Rey, F.A., de Groot, R.J., et al. (2019). Structural basis for human coronavirus attachment to sialic acid receptors. Nat. Struct. Mol. Biol. *26*, 481–489.

Vabret, N., Britton, G.J., Gruber, C., Hegde, S., Kim, J., Kuksin, M., Levantovsky, R., Malle, L., Moreira, A., and Park, M.D. (2020). Immunology of COVID-19: current state of the science. Immunity *52*, 910–941.

Van Zundert, G., Rodrigues, J., Trellet, M., Schmitz, C., Kastritis, P., Karaca, E., Melquiond, A., van Dijk, M., De Vries, S., and Bonvin, A. (2016). The HADDOCK2. 2 web server: user-friendly integrative modeling of biomolecular complexes. J. Mol. Biol. *428*, 720–725.

Varshney, A.K., Wang, X., Cook, E., Dutta, K., Scharff, M.D., Goger, M.J., and Fries, B.C. (2011). Generation, characterization, and epitope mapping of neutralizing and protective monoclonal antibodies against staphylococcal enterotoxin B-induced lethal shock. J. Biol. Chem. *286*, 9737–9747.

Verdoni, L., Mazza, A., Gervasoni, A., Martelli, L., Ruggeri, M., Ciuffreda, M., Bonanomi, E., and D'Antiga, L. (2020). An outbreak of severe Kawasaki-like disease at the Italian epicentre of the SARS-CoV-2 epidemic: an observational cohort study. Lancet *395*, 1771–1778.

Walls, A.C., Park, Y.-J., Tortorici, M.A., Wall, A., McGuire, A.T., and Veesler, D. (2020). Structure, function, and antigenicity of the SARS-CoV-2 spike glycoprotein. Cell *180*, 281–292.

Watanabe, Y., Allen, J.D., Wrapp, D., McLellan, J.S., and Crispin, M. (2020). Site-specific glycan analysis of the SARS-CoV-2 spike. Science *369*, 330–333.

Waterhouse, A., Bertoni, M., Bienert, S., Studer, G., Tauriello, G., Gumienny, R., Heer, F.T., de Beer, T.A.P., Rempfer, C., and Bordoli, L. (2018). SWISS-MODEL: homology modelling of protein structures and complexes. Nucleic Acids Res. *46*, W296–W303.

Woo, H., Park, S.-J., Choi, Y.K., Park, T., Tanveer, M., Cao, Y., Kern, N.R., Lee, J., Yeom, M.S., Croll, T.I., et al. (2020). Developing a fully glycosylated full-Length SARS-CoV-2 spike protein model in a viral membrane. J. Phys. Chem. B *124*, 7128–7137.

Wrapp, D., Wang, N., Corbett, K.S., Goldsmith, J.A., Hsieh, C.L., Abiona, O., Graham, B.S., and McLellan, J.S. (2020). Cryo-EM structure of the 2019-nCoV spike in the prefusion conformation. Science *367*, 1260–1263.

Xue, L.C., Rodrigues, J.P., Kastritis, P.L., Bonvin, A.M., and Vangone, A. (2016). PRODIGY: a web server for predicting the binding affinity of protein–protein complexes. Bioinformatics *32*, 3676–3678.

Yan, R., Zhang, Y., Li, Y., Xia, L., Guo, Y., and Zhou, Q. (2020). Structural basis for the recognition of SARS-CoV-2 by full-length human ACE2. Science *367*, 1444–1448.

Yuan, M., Wu, N.C., Zhu, X., Lee, C.D., So, R.T.Y., Lv, H., Mok, C.K.P., and Wilson, I.A. (2020). A highly conserved cryptic epitope in the receptor binding domains of SARS-CoV-2 and SARS-CoV. Science *368*, 630–633.

Zhang, Y., and Skolnick, J. (2005). The protein structure prediction problem could be solved using the current PDB library. Proc. Natl. Acad. Sci. U S A *102*, 1029–1034.

Zhou, D., Duyvesteyn, H.M., Chen, C.-P., Huang, C.-G., Chen, T.-H., Shih, S.-R., Lin, Y.-C., Cheng, C.-Y., Cheng, S.-H., Huang, Y.-C., et al. (2020a). Structural basis for the neutralization of SARS-CoV-2 by an antibody from a convalescent patient. Nat. Struct. Mol. Biol. *27*, 950–958.

Zhou, H., Chen, X., Hu, T., Li, J., Song, H., Liu, Y., Wang, P., Liu, D., Yang, J., and Holmes, E.C. (2020b). A novel bat coronavirus closely related to SARS-CoV-2 contains natural insertions at the S1/S2 cleavage site of the spike protein. Curr. Biol. *30*, 2196–2203.

Zost, S.J., Gilchuk, P., Case, J.B., Binshtein, E., Chen, R.E., Nkolola, J.P., Schäfer, A., Reidy, J.X., Trivette, A., Nargi, R.S., et al. (2020). Potently neutralizing and protective human antibodies against SARS-CoV-2. Nature *584*, 443–449.

STAR★METHODS

KEY RESOURCES TABLE

REAGENT or RESOURCE	SOURCE	IDENTIFIER
Antibodies		
6D3 IgG2b	Stony Brook University, New York	N/A
InVivoMab mouse IgG2b isotype control	BioXcell	Cat#BE0086
mouse anti-dsRNA [J2] antibody	Absolute Antibody	Cat#Ab01299-2.0
Goat anti-Mouse IgG (H+L) Cross-Adsorbed Secondary Antibody, Alexa Fluor 555	Thermo Fisher Scientific	Cat#A21422
Bacterial and Virus Strains		
SARS-CoV-2	BEI Resources of National Institute of Allergy and Infectious Diseases (NIAID)	Isolate USA-WA1/2020
Chemicals, Peptides, and Recombinant Proteins		
DAPI (4',6-Diamidino-2-Phenylindole, Dihydrochloride)	Life Technologies	Cat#D1306
Penicillin-Streptomycin (10,000 U/mL)	Gibco	Cat#15140122
Deposited Data		
Antibody-Spike complexes see Table 1	Protein Data Bank (PDB)	N/A
SARS-CoV-2 Spike with one chain in up state	(Wrapp et al., 2020)	PDB: 6VSB
SARS-CoV-2 Spike in down state	(Walls et al., 2020)	PDB: 6VXX
HCoV-OC43 Spike in down state	(Tortorici et al., 2019)	PDB: 6NZK
Furin	(Dahms et al., 2016)	PDB: 5JMO
SARS-CoV-2 glycosylated Spike protein model	(Woo et al., 2020)	https://charmm-gui.org/?doc=archive&lib=covid19
Antibodies 6D3 and 14G8 bound to SEB	(Dutta et al., 2015)	PDB: 4RGN
Antibody 20B1 bound to SEB	(Dutta et al., 2015)	PDB: 4RGM
Human TMPRSS2 homology model	This paper	https://zenodo.org/record/4667694#.YGz7DOhKhPZ
SARS-CoV-2 Spike bound to TMPRSS2	This paper	https://zenodo.org/record/4667694#.YGzUgOhKhPY
SARS-CoV-2 Spike bound to furin	This paper	https://zenodo.org/record/4667694#.YGzUgOhKhPY
Ab 6D3 bound to SARS-CoV-2 Spike in one up state	This paper	https://zenodo.org/record/4667694#.YGzUgOhKhPY
Ab 6D3 bound to SARS-CoV-2 Spike in down state	This paper	https://zenodo.org/record/4667694#.YGzUgOhKhPY
Ab 6D3 bound to HCoV-OC43 Spike in down state	This ppaer	https://zenodo.org/record/4667694#.YGzUgOhKhPY
Experimental Models: Cell Lines		
Vero-E6	ATCC	Cat#CRL-1586
Software and Algorithms		
ClusPro	(Kozakov et al., 2017)	https://cluspro.bu.edu/
SWISS-MODEL	(Waterhouse et al., 2018)	https://swissmodel.expasy.org/interactive
PRODIGY	(Xue et al., 2016)	https://bianca.science.uu.nl//prodigy/
PyMOL	(DeLano, 2002)	https://pymol.org/2/
HADDOCK 2. 4	(Van Zundert et al., 2016)	https://bianca.science.uu.nl/haddock2.4/
Clustal Omega	(Sievers et al., 2011)	https://www.ebi.ac.uk/Tools/msa/clustalo/
Prism	GraphPad	https://www.graphpad.com/scientific-software/prism/
BZ-X700 Analysis Software	Keyence	https://www.keyence.com/landing/microscope/lp_fluorescence.jsp
Other		
Eagle's Minimum Essential Medium (MEM)	Corning	Cat#10009CV
Regular Fetal Bovine Serum	Corning	Cat#35010CV
Goat Serum	Cell Signaling	Cat#5425S
Normal Donkey Serum	Jackson ImmunoResearch	Cat#017-000-121
BZ-X710 Fluorescence Microscope	Keyence	Model#BZ-X710

RESOURCE AVAILABILITY

Lead contact

All requests should be directed to and will be fulfilled by the Lead Contact, Ivet Bahar (bahar@pitt.edu).

Materials availability

This study did not generate new unique reagents.

Data and code availability

The following are accessible via zenodo.org via the https://zenodo.org/record/4667694#.YGzUgOhKhPY

File Name: Homology model Human_TMPRSS2_on_PDB5CE1.pdb

Description: A pdb file of the homology model of human TMPRSS2.

File Name: SARS-CoV-2 spike_TMPRSS2_refined_model.pdb

Description: A pdb file of the representative refined docking model of SARS-CoV-2 Spike bound to TMPRSS2.

File Name: SARS-CoV2 spike_furin_refined_model.pdb

Description: A pdb file of the representative refined docking model of SARS-CoV-2 Spike bound to furin.

File Name: Antibody 6D3 bound to SARS-CoV-2 Spike on 6VSB.pdb

Description: A pdb file of the representative docking model of Ab 6D3 bound to SARS-CoV-2 Spike with one RBD in the up state.

File Name: Antibody 6D3 bound to SARS-CoV-2 Spike in down states.pdb

Description: A pdb file of the representative docking model of Ab 6D3 bound to SARS-CoV-2 Spike with three RBDs in the down state.

File Name: Antibody 6D3 bound to HCoV OC43 on 6NZK.pdb

Description: A pdb file of the representative docking model of Ab 6D3 bound to HCoV-OC43 Spike with three RBDs in the down state.

EXPERIMENTAL MODEL AND SUBJECT DETAILS

Cell line: Monkey (species: *Cercopithecus aethiops*) kidney epithelial cell line; Vero-E6 [VERO C1008 (ATCC@ CRL-1586^{TM})], was obtained from ATCC. Cells were cultured at 37°C with 5% CO_2 in EMEM growth media with 10% fetal bovine serum and 100 units/ml penicillin.

METHOD DETAILS

In vitro viral inhibition assays

SARS-CoV-2 viral assays were performed in UCLA BSL3 high containment facility, following previous procedure(Garcia et al., 2020). SARS-CoV-2 Isolate USA-WA1/2020 was obtained from BEI Resources of National Institute of Allergy and Infectious Diseases (NIAID). Mouse Fab 6D3 (IgG2b) was generated as(Varshney et al., 2011). Vero-E6 cells were plated in 96-well plates ($5x10^3$ cells/well). 6D3 IgG2b or mouse IgG2b isotype control (Bio X Cell) were incubated with virus (100 PFU/well) for 1 hour at room temperature prior to addition to Vero-E6 cells. After 48 hours post-infection the cells were fixed with methanol for 30-60 minutes in -20 °C. Cells were washed 3 times with PBS and permeabilized using blocking buffer (0.3% Triton X-100, 2% BSA, 5% Goat Serum, 5% Donkey Serum in 1 X PBS) for 1 hour at room temperature. Subsequently, cells were incubated with mouse anti-dsRNA antibody (Absolute Antibody, 1:200) or anti-SARS-CoV-2 spike antibody (Sino Biological, 1:200) at 4°C overnight. Cells were then washed 3 times with PBS and incubated with fluorescence conjugated secondary antibody: Goat anti-mouse IgG Secondary Antibody, Alexa Fluor 555 (Fisher Scientific, 1:1000) for 1 hour at room temperature. Nuclei were stained with DAPI (4',6-Diamidino-2-Phenylindole, Dihydrochloride) (Life Technologies) at a dilution of 1:5000 in PBS for 10 minutes. Cells were analyzed by fluorescence microscopy. Images were obtained using a Biorevo BZ-X710 (Keyence) microscope and software.

Structural data for SARS-CoV-2, human TMPRSS2 and furin

SARS-CoV-2 (residues A27-D1146; UniProt ID: P0DTC2) spike models were generated using SWISS-MODEL (Waterhouse et al., 2018), based on the resolved SARS-CoV-2 Spike glycoprotein structures of SARS-CoV-2 in different conformational states (PDBs: 6VSB (Wrapp et al., 2020) and 6VXX (Walls et al., 2020)). The missing loops in the crystal structures, were built using the well-established libraries of backbone fragments (Zhang and Skolnick, 2005) and constraint space *de novo* reconstruction of the backbone segments (Peitsch, 1995). The catalytic domain of human TMPRSS2 (residues N146-D491; UniProt ID: O15393) was constructed using SWISS-MODEL (Waterhouse et al., 2018), based on the crystal structure of serine protease hepsin (PDB: 5CE1). A crystal structure of human furin (Y110-A408; P09958) was used as is (PDB: 5JMO) (Dahms et al., 2016).

Generation and assessment of SARS-CoV-2 Spike and protease complex models

To investigate priming of the S1/S2 site of SARS-CoV-2 Spike, we performed protein-protein docking analysis of TMPRSS2 or furin with SARS-CoV-2 Spike in the pre-fusion state. Using docking software ClusPro (Kozakov et al., 2017), we constructed *in silico* a

series of SARS-CoV-2 Spike and protease complexes. SARS-CoV-2 Spike was set as receptor and protease as ligand. Residues in the proximity of the cleavage site from SARS-CoV-2 Spike (T676 to V687) were set as attractor sites of receptor, and the catalytic residues from TMPRSS2 (H296, D345 and S441) or furin (D153, H194 and S368) were set as attractor sites for ligand. For each complex, we obtained 30 clusters of conformations, upon clustering ~800 models generated by ClusPro. The clusters were rank-ordered by cluster size (Kozakov et al., 2017) as recommended, and representative members from top-ranking clusters were further examined and refined Mainly, protein-protein binding free energies were calculated using PRODIGY (Xue et al., 2016); and mutagenesis and sculpting wizards in PyMOL 2.3.0 (Open Source version) (DeLano, 2002) were used to interactively refine rotamers and interactions, respectively.

Monoclonal antibodies binding to SARS-CoV-2 Spike

SEB-associated monoclonal antibodies 14G8, 6D3 and 20B1 were taken from the crystal structures of SEB bound to two neutralizing Abs, 14G8 and 6D3 (PDB: 4RGN), and one neutralizing Ab, 20B1 (PDB: 4RGM). SARS-CoV-2 S-associated neutralizing Abs were taken from the crystal structures listed in Table 1. Ab-binding poses were predicted using protein-protein docking module in ClusPro (Kozakov et al., 2017) where SARS-CoV-2 spike was set as the receptor and 6D3 as the ligand. Computations repeated with the antibody mode of ClusPro confirmed the S1/S2 cleavage site to be most favorable binding site for mAb 6D3. All docking simulations were performed using ClusPro default parameters.

Model refinement and binding affinity calculations

Selective protease-Spike and mAb-Spike complexes were further refined using the refinement protocol implemented in the webserver HADDOCK 2.4 (Van Zundert et al., 2016). Refinement was performed by MD energy minimization following the protocol and default parameters provided by the webserver. Binding free energies were evaluated using the inter-residue contact-based method accessible in the webserver PRODIGY (Xue et al., 2016). The standard deviations of binding free energy were estimated based on multiple binding poses taken from docking simulations and model refinement.

Sequence alignment

Multiple sequence alignment of the variable heavy chain domain of anti-SEB Abs (6D3, 14G8 and 20B1) and anti-SARS-CoV-2 S Abs were generated by Clustal Omega (Sievers et al., 2011).

QUANTIFICATION AND STATISTICAL ANALYSIS

For viral inhibition assays

Quantification of immunofluorescence images was performed manually, blinded to the conditions. Five images per well were quantified and the average calculated. n = 3 technical replicates (wells) per condition. Data is presented as mean +/- standard error of the mean and is representative of three independent experiments. Data were analyzed by t test (6D3 vs. isotype control) with multiple testing correction (Benjamini, Krieger and Yekutieli FDR test) using GraphPad Prism software. No methods were used to test the assumptions of the statistical approach. Statistical analysis details are found in the methods description, results and figure captions.